Impedance Modeling and Stability Analysis of Grid-tied Universal Droop Control Inverter

Mohammad Amin
Department of Electric Power Engineering
Norwegian University of Science and Technology
Trondheim-7491, Norway
Email: mohammad.amin@ntnu.no

Qing-Chang Zhong
Dept. of Electrical and Computer Engineering
Illinois Institute of Technology
Chicago, IL 60616, USA
Email: zhongqc@iit.edu

***Abstract*—This paper presents an impedance modeling and small-signal stability analysis of the grid-tied Universal Droop Control (UDC) inverter. The dq-impedance model of the UDC inverter is derived analytically, which is verified by simulation. The impedance model is used to determine the stability of the grid-tied UDC inverter. Simulation and experimental results are provided to further verify the theoretical analysis.**

***Index Terms*—Small-signal analysis, impedance modeling, universal droop control, impedance-based stability.**

I. Introduction

Distributed generation (DG) based on renewable energy such as solar, wind, is increasing significantly. The controllers of the DG inverters should comply with the grid code requirement, i.e., having the function to regulate the voltage and frequency. The virtual synchronous machine based inverter control has this functionality [1]–[5]. Recently, another type of inverter control, known as Universal Droop Control (UDC) is proposed in [6], which also has the voltage and frequency regulating capability. Both the frequency droop and the voltage droop control are embedded to regulate the voltage and the frequency. The UDC has been tested for the different types of the inverter impedance such as the capacitive, resistive and inductive impedance inverter [6], and it is shown that this technology is universal regardless inverter impedance type and is applicable to inverters having an impedance angle between $-\pi/2$ rad and $\pi/2$ rad. In [7], it is shown that a self-synchronization mechanism can be embedded with the UDC to form a self-synchronized UDC. Therefore, a dedicated synchronization unit such as a phase-locked-loop (PLL) is no longer required for synchronization purpose. The UDC inverter ensures the load sharing naturally in the same way as the conventional generator does [8]. Moreover, the UDC facilitates the DG inverters to operate in both the grid-connected mode as well as the islanded mode [6], [8].

The UDC inverter is relatively easy in integrating distributed generation; however, determining the stability of UDC inverter is not easy due to non-linearity of the controller. In [9], a line-frequency-averaged small-signal model of the UDC inverter is derived for the purpose of parameter design, however, a detailed stability study is missing. This paper focuses on filling this research gap by studying the stability analysis of the UDC inverter. The stability analysis can be carried out by deriving a state-space model and studying the eigenvalues [10]–[12], nonlinear method [13], adopting the impedance-based analysis [14]–[16]. The impedance-based analysis is a relatively easy method to predict the stability of the power electronics system, therefore, the impedance-based method is adopted in this study. The impedance model of the UDC inverter is derived analytically in the dq-frame. The derived model is verified by simulation, then the derived model is used to determine the stability of the grid-connected UDC inverter. Simulation and experimental results are provided to verify the theoretical analysis. It is also shown that using this method, it is possible to redesign the parameters to reinforce the instability of the system.

II. DQ-Impedance Modeling of the UDC Inverter

The electrical circuit of an inverter for analytical modeling is shown in Fig. 1(a) where L_c and R_c are the total series inductance and resistance between the inverter and the point of common coupling, C_f is the filter capacitance, L_g and R_g are the equivalent inductance and resistance of the grid. The currents and voltages are indicated in Fig. 1(a).

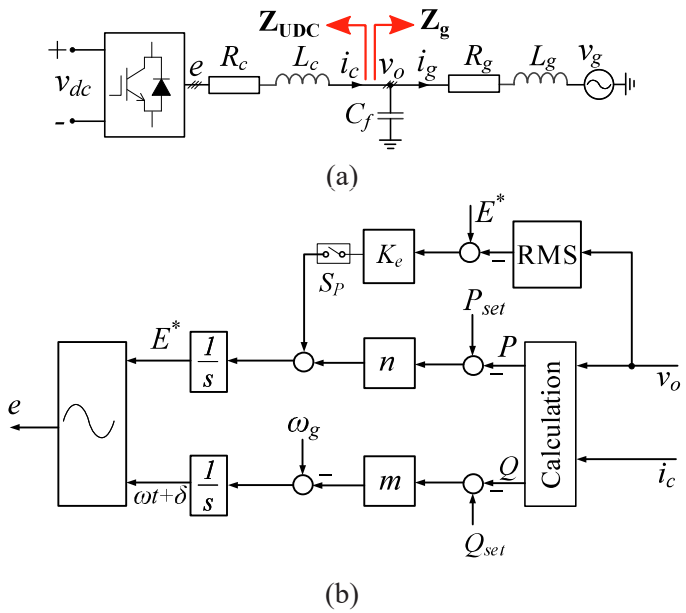

Fig. 1. UDC inverter, (a) power part and (b) controller part.

A. Overview of the UDC

The active power and the reactive power send by the inverter can be given by

$$P = \frac{3EV_o\cos\delta - 3V_o^2}{Z}\cos\theta + \frac{3EV_o\sin\delta\sin\theta}{Z} \quad (1)$$

$$Q = \frac{3EV_o\cos\delta - 3V_o^2}{Z}\sin\theta - \frac{3EV_o\sin\delta\cos\theta}{Z} \quad (2)$$

where δ is the phase difference between the inverter voltage, e and the capacitor voltage, v_o; Z and θ are the impedance magnitude and angle, respectively; E and V_o are the RMS value of e and v_o, respectively as shown in Fig. 1(a). It is assumed that Z is dominantly resistive, i.e., $\theta \approx 0$ and δ is very small. Thus, (1) and (2) can be rewritten by

$$P = \frac{3E - 3V_o}{R_c}V_o \quad (3)$$

$$Q = -\frac{3EV_o}{R_c}\delta \quad (4)$$

which leads to

$$P \sim V_o \text{ and } Q \sim -\delta \quad (5)$$

droop relationship. Based on these relationships, the UDC for inverters is proposed as [7]

$$E = \frac{1}{s}\left(n\left(P_{set} - P\right) + S_P K_e\left(E^* - V_o\right)\right) \quad (6)$$

$$\omega = \omega_g - m(Q_{set} - Q) \quad (7)$$

where E^* is the reference RMS value of the output voltage; ω_g is the nominal frequency of the grid; and n and m are the voltage droop and frequency droop coefficient, respectively; P_{set} and Q_{set} are the reference active and reactive power; K_e and K are positive gains; and S_P is switching state, 1 for ON and 0 for OFF. The UDC is shown in Fig. 1(b).

Eqns. (1) and (2) can be rewritten as

$$\begin{bmatrix} P \\ Q \end{bmatrix} = \begin{bmatrix} \cos\theta & -\sin\theta \\ \sin\theta & \cos\theta \end{bmatrix} \begin{bmatrix} \frac{3EV_o\cos\delta - 3V_o^2}{R_c} \\ -\frac{3EV_o}{R_c}\sin\delta \end{bmatrix}. \quad (8)$$

The eigenvalues of $\begin{bmatrix} \cos\theta & -\sin\theta \\ \sin\theta & \cos\theta \end{bmatrix}$ are $\cos\theta \pm j\sin\theta$, of which the real part $\cos\theta$ is positive for any output impedance with $\theta \in (-\pi/2, \pi/2)$. Hence, the relationship (5) holds for $\theta \in (-\pi/2, \pi/2)$. This means the controller is universal regardless of the impedance type of the inverter and can be applied to any inverters having an impedance angle between $-\pi/2$ rad and $\pi/2$ rad.

B. Analytical DQ-Impedance Model Derivation

The impedance model of the inverter is derived in the dq-frame. The transformation of the three-phase quantity from stationary reference frame to the dq-frame is based on the amplitude-invariant Park transformation, with the d-axis aligned with the voltage vector v_o and q-axis leading the d-axis by 90^o. The dynamic equation of the inverter in the small-signal dq-frame can be written by

$$\tilde{\mathbf{v}}^{\mathbf{s}}_{\mathbf{odq}} = \tilde{\mathbf{e}}^{\mathbf{s}}_{\mathbf{dq}} - \mathbf{Z_{con}}\tilde{\mathbf{i}}^{\mathbf{s}}_{\mathbf{cdq}}, \quad (9)$$

where

$$\mathbf{Z_{con}} = \begin{bmatrix} sL_c + R_c & -\omega_g L_c \\ \omega_g L_c & sL_c + R_c \end{bmatrix},$$

$\tilde{\mathbf{v}}^{\mathbf{s}}_{\mathbf{odq}} = \begin{bmatrix} \tilde{v}^s_{od} & \tilde{v}^s_{oq} \end{bmatrix}^T$, $\tilde{\mathbf{e}}^{\mathbf{s}}_{\mathbf{dq}} = \begin{bmatrix} \tilde{e}^s_d & \tilde{e}^s_q \end{bmatrix}^T$, $\tilde{\mathbf{i}}^{\mathbf{s}}_{\mathbf{cdq}} = \begin{bmatrix} \tilde{i}^s_{cd} & \tilde{i}^s_{cq} \end{bmatrix}^T$. The superscript "$s$" is used to represent the variable in the system dq-frame and the bold font is used to represent variables in the matrix form. The impedance of the UDC inverter can be obtained by dividing the capacitor phase-voltage $\tilde{\mathbf{v}}^{\mathbf{s}}_{\mathbf{odq}}$ by the inverter current $\tilde{\mathbf{i}}^{\mathbf{s}}_{\mathbf{cdq}}$. In order to obtain the impedance of the inverter, $\tilde{\mathbf{e}}^{\mathbf{s}}_{\mathbf{dq}}$ in (9) needs to be represented in terms of $\tilde{\mathbf{v}}^{\mathbf{s}}_{\mathbf{odq}}$ and $\tilde{\mathbf{i}}^{\mathbf{s}}_{\mathbf{cdq}}$.

The transformation from the stationary reference to the system dq-frame can be described as

$$v_{o\alpha} + jv_{o\beta} = e^{j\theta_g}\left(v^s_{od} + jv^s_{oq}\right) \quad (10)$$

and the transformation from the stationary reference to the inverter dq-frame can be described as

$$v_{o\alpha} + jv_{o\beta} = e^{j\delta}\left(v^c_{od} + jv^c_{oq}\right). \quad (11)$$

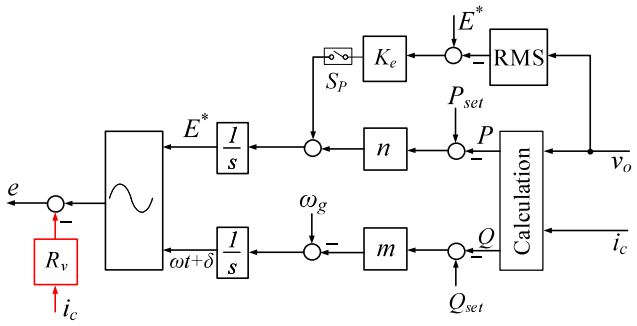

Fig. 2. UDC with the virtual resistance R_v.

Thus, the relation between the system and inverter dq-frame voltage can be written by

$$v_{od}^c + jv_{oq}^c = e^{-j\Delta\delta}\left(v_{od}^s + jv_{oq}^s\right) \tag{12}$$

where $\Delta\delta = \delta - \theta_g$. In small-signal form, the relation between these two frames voltage can be given by

$$\tilde{\mathbf{v}}_{\mathbf{odq}}^{\mathbf{c}} = \mathbf{G}_{\boldsymbol{\delta}}\tilde{\mathbf{v}}_{\mathbf{odq}}^{\mathbf{s}} + \mathbf{G_{d1}}\boldsymbol{\Delta}\tilde{\boldsymbol{\delta}} \tag{13}$$

where $\boldsymbol{\Delta}\tilde{\boldsymbol{\delta}} = \begin{bmatrix} \Delta\tilde{\delta} & 0 \end{bmatrix}^T$ and

$$\mathbf{G}_{\boldsymbol{\delta}} = \begin{bmatrix} \cos\Delta\delta_n & -\sin\Delta\delta_n \\ \sin\Delta\delta_n & \cos\Delta\delta_n \end{bmatrix}$$

$$\mathbf{G_{d1}} = \begin{bmatrix} -V_{od}^s\sin\Delta\delta_n - V_{oq}^s\cos\Delta\delta_n & 0 \\ -V_{od}^s\cos\Delta\delta_n + V_{oq}^s\sin\Delta\delta_n & 0 \end{bmatrix}.$$

Similarly, the relation between the system and inverter dq-frame current and voltage can be written as

$$\tilde{\mathbf{i}}_{\mathbf{cdq}}^{\mathbf{c}} = \mathbf{G}_{\boldsymbol{\delta}}\tilde{\mathbf{i}}_{\mathbf{cdq}}^{\mathbf{s}} + \mathbf{G_{d2}}\boldsymbol{\Delta}\tilde{\boldsymbol{\delta}} \tag{14}$$

$$\tilde{\mathbf{e}}_{\mathbf{dq}}^{\mathbf{c}} = \mathbf{G}_{\boldsymbol{\delta}}\tilde{\mathbf{e}}_{\mathbf{dq}}^{\mathbf{s}} + \mathbf{G_{d3}}\boldsymbol{\Delta}\tilde{\boldsymbol{\delta}} \tag{15}$$

where

$$\mathbf{G_{d2}} = \begin{bmatrix} -I_{cd}^s\sin\Delta\delta_n - I_{cq}^s\cos\Delta\delta_n & 0 \\ -I_{cd}^s\cos\Delta\delta_n + I_{cq}^s\sin\Delta\delta_n & 0 \end{bmatrix}$$

$$\mathbf{G_{d3}} = \begin{bmatrix} -E_d^s\sin\Delta\delta_n - E_{oq}^s\cos\Delta\delta_n & 0 \\ -E_d^s\cos\Delta\delta_n + E_{oq}^s\sin\Delta\delta_n & 0 \end{bmatrix}.$$

The active power and the reactive power can be calculated in the inverter dq-frame as

$$P = \frac{3}{2}\left(v_{od}^c i_{cd}^c + v_{oq}^c i_{cq}^c\right) \tag{16}$$

$$Q = \frac{3}{2}\left(-v_{od}^c i_{cq}^c + v_{oq}^c i_{cd}^c\right) \tag{17}$$

The frequency of the inverter from (7) can be given in the small-signal form by

$$\tilde{\omega} = \tilde{\omega}_g - m\left(\tilde{Q}_{set} - \tilde{Q}\right). \tag{18}$$

As shown in Fig. 1(b), the phase of the output voltage of the UDC is obtained by applying Laplace transformation to (7). In the small-signal form, the phase can be given by

$$\Delta\tilde{\delta} = \frac{1}{s}(\tilde{\omega}_g - m(\tilde{Q}_{set} - \tilde{Q})). \tag{19}$$

Inserting (17) in (19), it can be given in the small-signal form,

$$\boldsymbol{\Delta}\tilde{\boldsymbol{\delta}} = \overbrace{\frac{1.5m}{s}\begin{bmatrix} -I_{cq}^c & I_{cd}^c \\ 0 & 0 \end{bmatrix}}^{\mathbf{G_{d4}}}\tilde{\mathbf{v}}_{\mathbf{odq}}^{\mathbf{c}} + \overbrace{\frac{1.5m}{s}\begin{bmatrix} V_{oq}^c & -V_{od}^c \\ 0 & 0 \end{bmatrix}}^{\mathbf{G_{d5}}}\tilde{\mathbf{i}}_{\mathbf{cdq}}^{\mathbf{c}}. \tag{20}$$

Now inserting (13) and (14) in (20), it can be obtained,

$$\boldsymbol{\Delta}\tilde{\boldsymbol{\delta}} = \mathbf{G}_{\mathbf{d}}^{\mathbf{v}}\tilde{\mathbf{v}}_{\mathbf{odq}}^{\mathbf{s}} + \mathbf{G}_{\mathbf{d}}^{\mathbf{i}}\tilde{\mathbf{i}}_{\mathbf{cdq}}^{\mathbf{s}} \tag{21}$$

where

$$\mathbf{G}_{\mathbf{d}}^{\mathbf{v}} = \left(\mathbf{I} - \mathbf{G_{d4}}\mathbf{G_{d1}} - \mathbf{G_{d5}}\mathbf{G_{d2}}\right)^{-1}\mathbf{G_{d4}}\mathbf{G}_{\boldsymbol{\delta}} \tag{22}$$

$$\mathbf{G}_{\mathbf{d}}^{\mathbf{i}} = \left(\mathbf{I} - \mathbf{G_{d4}}\mathbf{G_{d1}} - \mathbf{G_{d5}}\mathbf{G_{d2}}\right)^{-1}\mathbf{G_{d5}}\mathbf{G}_{\boldsymbol{\delta}} \tag{23}$$

and $\mathbf{I}$ is a 2x2 identity matrix.

Inverters are connected to the grid by using inductive elements in series and capacitive elements in parallel (L, LC, LCL, etc.), thus, the inverter impedance is not resistive. Therefore, a virtual resistance, R_v is added in series as shown in Fig. 2 to make the impedance dominantly resistive. The reference voltage from the UDC in the inverter dq-frame can be given by

$$\mathbf{e}_{\mathbf{dq}}^{\mathbf{c}} = \overbrace{\begin{bmatrix} H_{pwm} & 0 \\ 0 & H_{pwm} \end{bmatrix}}^{G_{PWM}}\left(-\begin{bmatrix} R_v & 0 \\ 0 & R_v \end{bmatrix}\tilde{\mathbf{i}}_{\mathbf{cdq}}^{\mathbf{c}} + \begin{bmatrix} \frac{1}{s}\left(m\left(P^* - P\right) + K_e\left(E^* - V_o\right)\right) \\ 0 \end{bmatrix}\right) \tag{24}$$

where H_{pwm} is the PWM delay and can be modeled as $H_{pwm} = 1/(1 + 1.5sT_{sw})$ and $T_{sw} = 1/f_{sw}$, f_{sw} is the switching frequency. Assume that the inverter operates in $P-$set mode. First, inserting (16) in (24), and then inserting (13), (14), (15) and (21), the inverter voltage can be given in the small-signal form in the system dq-frame as

$$\tilde{\mathbf{e}}_{\mathbf{dq}}^{\mathbf{s}} = -\mathbf{G_C}\tilde{\mathbf{v}}_{\mathbf{odq}}^{\mathbf{s}} - \mathbf{G_D}\tilde{\mathbf{i}}_{\mathbf{cdq}}^{\mathbf{s}} \tag{25}$$

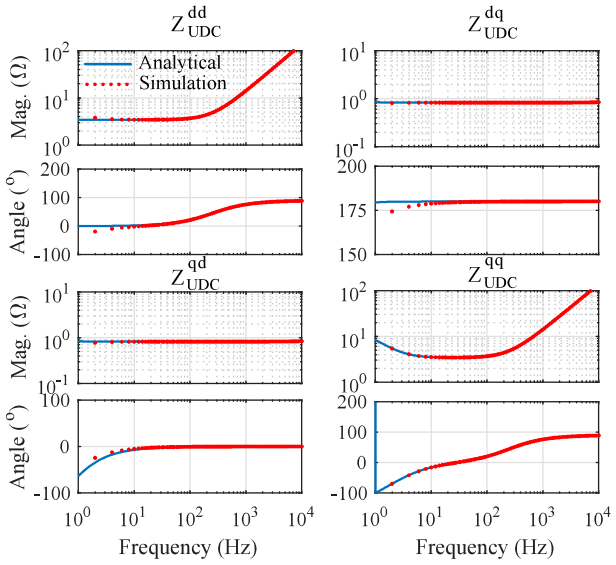

Fig. 3. Comparison of the impedance frequency response (the solid-line is from analytical model and points are from detailed simulation).

where

$$\begin{aligned}
\mathbf{G_C} &= \mathbf{G_\delta^{-1}G_A}\left(\mathbf{G_\delta}+\mathbf{G_{d1}G_d^v}\right)\\
&\quad +\mathbf{G_\delta^{-1}}\left(\mathbf{G_B G_{d2}}+\mathbf{G_{d3}}\right)\mathbf{G_d^v}\\
\mathbf{G_D} &= \mathbf{G_\delta^{-1}G_B}\left(\mathbf{G_\delta}+\mathbf{G_{d2}G_d^i}\right)\\
&\quad +\mathbf{G_\delta^{-1}}\left(\mathbf{G_A G_{d1}}+\mathbf{G_{d3}}\right)\mathbf{G_d^i}\\
\mathbf{G_A} &= \frac{1.5m}{s}G_{PWM}\begin{bmatrix} I_{cd}^c & I_{cq}^c \\ 0 & 0 \end{bmatrix}\\
\mathbf{G_B} &= \frac{1.5m}{s}G_{PWM}\begin{bmatrix} V_{od}^c & V_{oq}^c \\ 0 & 0 \end{bmatrix}\\
&\quad +G_{PWM}\begin{bmatrix} R_v & 0 \\ 0 & R_v \end{bmatrix}.
\end{aligned}$$

Now inserting (25) in (9), the dq-impedance model of the UDC inverter is obtained as

$$\mathbf{Z_{UDC}}(\mathrm{s}) = -\left(\mathbf{I}+\mathbf{G_C}\right)^{-1}\left(-\mathbf{Z_{con}}-\mathbf{G_D}\right). \qquad (26)$$

The impedance model derived analytically is verified by simulation. More detail about the dq-impedance measurement by simulation/experiment can be found in [17], [18]. The impedance frequency responses obtained analytically and by simulation are shown in Fig. 3. The inverter parameters are given in Table I. The solid line is representing the analytical impedance and points show the results from the simulation. Both analytical and simulation impedance magnitude and phase are in good agreement which validates the correctness of the derived impedance model. The d- and q-axis impedance show the resistive behavior at the fundamental frequency. The d-axis impedance is resistive up to 200 Hz. The q-axis impedance shows a negative impedance below 10 Hz.

TABLE I
PARAMETERS OF THE INVESTIGATED SYSTEM.

Parameters	Values
Rated apparent power, S_b	2000 VA
Rated voltage (L-L, RMS), V_o	208 V
Rated dc voltage,V_{dc}	400 V
Grid frequency, f_g	60 Hz
Inverter series inductance, L_c	2.2 mH
Inverter series resistance, R_c	0.6 Ω
Filter capacitance, C_f	22 μF

III. IMPEDANCE-BASED STABILITY ANALYSIS OF THE UDC INVERTER

When using the impedance-based stability analysis for a grid-connected inverter, the inverter is treated as a load [15], and the Generalized Nyquist Criterion (GNC) is applied to the impedance ratio between the grid-side impedance $\mathbf{Z_g}(\mathrm{s})$ and the inverter impedance $\mathbf{Z_{UDC}}(\mathrm{s})$ as

$$\mathbf{L}(\mathrm{s}) = \mathbf{Z_g}(\mathrm{s})\mathbf{Z_{UDC}^{-1}}(\mathrm{s}). \qquad (27)$$

As shown in Fig. 1(a), the capacitor and grid-side inductor of the LCL filter are assumed to be the part of the grid impedance. Using $\mathbf{Z_g}(\mathrm{s})$ and $\mathbf{Z_{UDC}}(\mathrm{s})$ and applying GNC to the impedance ratio $\mathbf{L}(\mathrm{s})$, the stability condition of the system can be predicted correctly.

The parameters of the inverter are given in Table I. The virtual resistance R_v is selected $3\,\Omega$ and $K_e = 15$. The active power and the reactive power of the inverter is set to 1800 W and 150 Var. Assume that the grid is strong with an short circuit ratio (SCR) of 5. Fig. 4(a) shows the GNC plot of the impedance ratio matrix $\mathbf{L}(\mathrm{s})$. As can be seen, none of the system's characteristic loci encircles the critical point (–1, $j0$), thus, the system will be stable.

Now the stability has been investigated for a lower value of the SCR. An additional inductor is added in series with the grid so that the SCR becomes 1.4. Fig. 4(b) system characteristics loci for this SCR. As can be seen, λ_2 encircles the point $(-1, j0)$ at frequency 1 Hz, the system is clearly unstable. If the system becomes unstable, different steps can be taken in order to improve the stability of the system. The practice is redesigning controller parameters in order to have a stable system. The parameters of the UDC are the droop coefficients m and n, virtual resistance R_v and the positive gain K_e. The droop coefficients m and n are selected based on the grid code requirement, therefore, it is not recommended

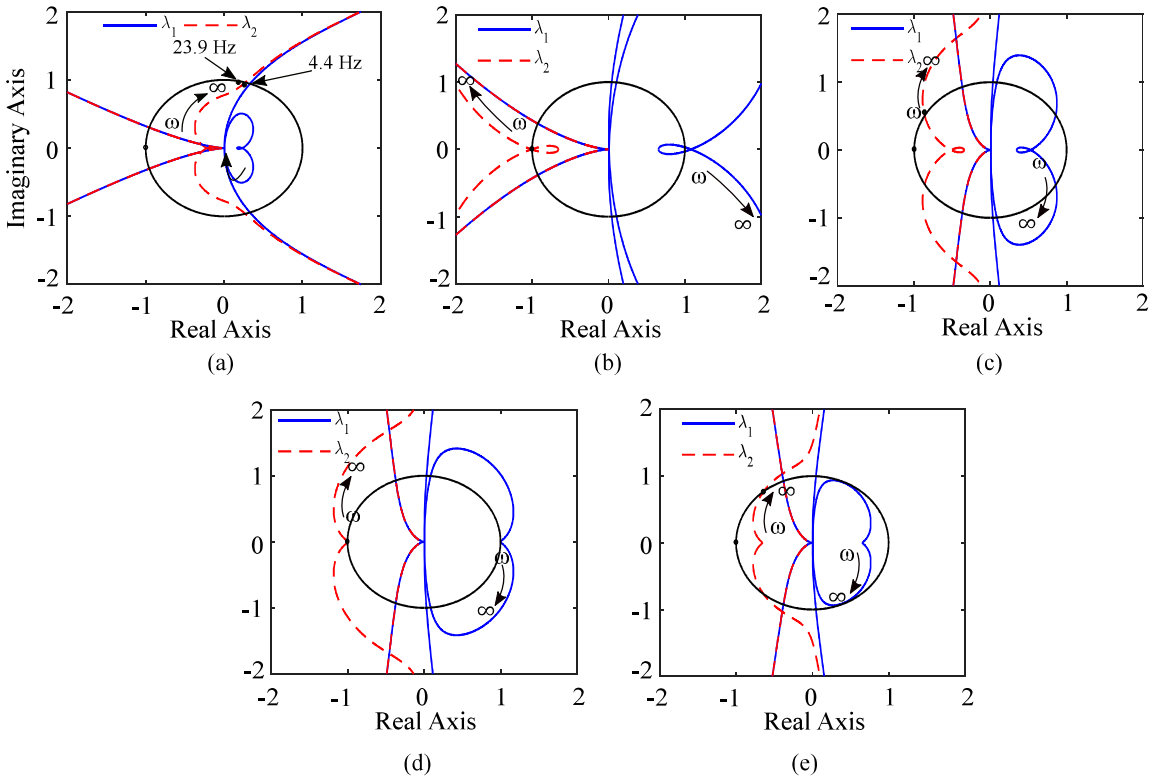

Fig. 4. GNC plot of the impedance ratio when (a) SCR= 5, (b) SCR= 1.4, unstable, (c) SCR=1.4, stable with redesigned parameter, (d) SCR= 1 and 60 % rated power, unstable and (d) SCR= 1, stable with redesigned parameter.

modifying these parameters. The virtual resistance R_v can be redesigned. In order to improve the stability, R_v is increased to 15 Ω. The stability analysis is carried out for the new value of R_v when the SCR= 1.4, and the GNC plot is shown in Fig. 4(c). Since for the new value of R_v, none of the characteristic loci encircles the point the $(-1, j0)$, the system is predicted to be stable.

The stability analysis is carried out for further lower value of the SCR. The grid SCR is reduced to 1 by adding more inductor in series with the grid, the stability analysis has been carried out. The system characteristic loci is shown in Fig. 4(d). As can be seen, λ_2 encircles the point $(-1, j0)$ for $R_v = 15$. Since one of the characteristic loci encircles the point $(-1, j0)$, the system is unstable. The analysis is carried out for 100 % rated power of the inverter. The analysis indicates that the inverter cannot send its full rated power when the SCR is 1. The stability analysis is carried out for 60 % of the rated power when the SCR= 1, the resulting GNC plot is shown in Fig. 4(e). For this lower value of the power, none of the characteristic loci encircles the point $(-1, j0)$, and hence, the system is predicted to be stable for 60 % of the rated power.

IV. Simulation and Experimental Results

In order to verify the above theoretical analysis, simulations and experiments are carried out. The parameters of the converter system are given in the Table I.

A. Simulation

A three-phase UDC inverter is implemented in MATLAB/Simulink association with Sim Power System block set. The grid is assumed to be a strong grid with an SCR of 5 and $R_v = 3\,\Omega$. Simulation is carried out for this grid condition and simulation results is shown in Fig. 5(a). The simulation is started at $t = 0$ s, and at $t = 1$ s, the real power and the reactive power commands are set to $P_{set} = 1800$ W and $Q_{set} = 150$ Var. The inverter quickly responded to the commands accurately. The overall system performance is satisfactory.

A simulation is carried out for a weak grid condition. The grid inductance has been increased purposely so that the SCR becomes 1.4. Simulation result for this grid condition is shown in Fig. 5(b). The system is unstable. It has a low-frequency oscillation at around 1 Hz as predicted in the stability analysis. Now R_v is increased to 15 Ω as discussed in the impedance-based analysis. The

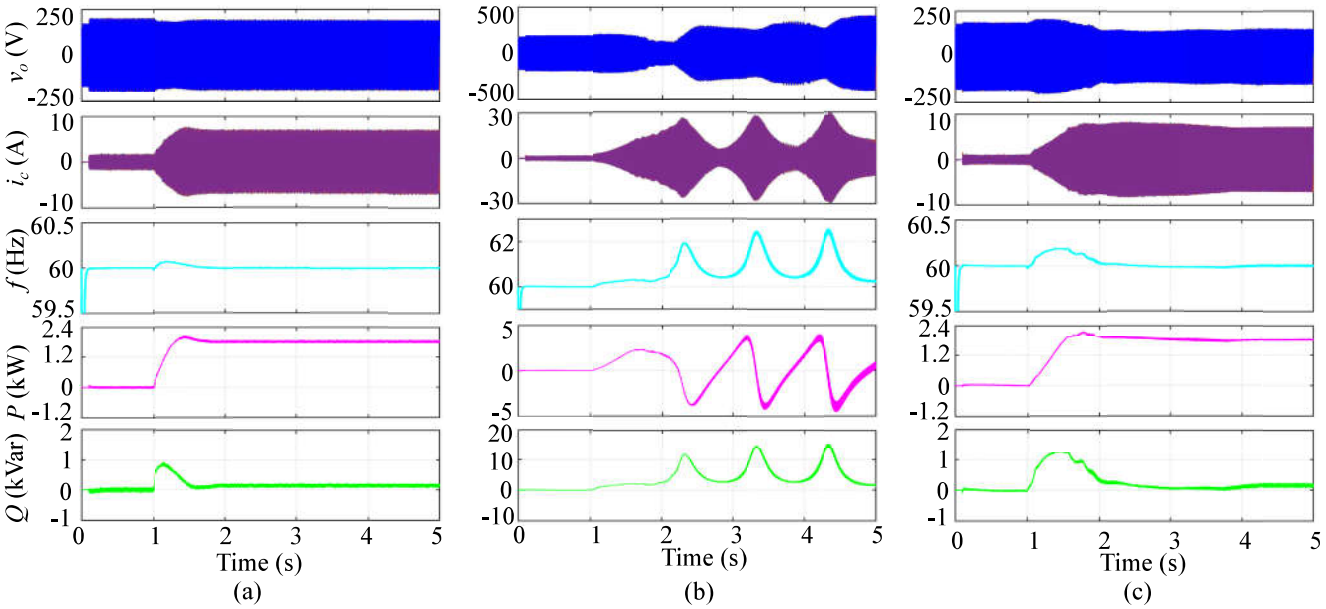

Fig. 5. Simulation results for different scenarios of the grid condition: (a) strong grid, stable system (b) weak grid, unstable system and (c) weak grid, stable system with redesigned parameter.

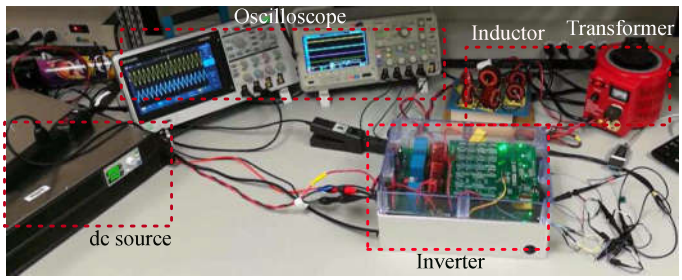

Fig. 6. The experimental set-up. .

simulation results are shown in Fig. 5(c). As predicted in the impedance-based analysis, the system is stable for a weak grid condition.

B. Experiment

In order to further verify the theoretical analysis, experiments are carried out for an equivalent single-phase system. The experimental setup is shown in Fig. 6. First, it is assumed that the grid is strong. Fig. 7(a) shows the experimental results when $R_v = 3$. The PWM of the inverter is turned on at $t = 0.4$ s. The real power and reactive power commands are set to $P_{set} = 1800/3 = 600$ W and $Q_{set} = 150/3 = 50$ Var at $t = 1$ s. The inverter quickly responded to the commands accurately. The system is stable.

Now a 19.3-mH inductor is connected to the grid to make the grid weak. All the controller parameters remain the same. An experiment is carried out and experimental results are shown in Fig. 7(b). The inverter intends to respond accordingly, however, the voltage is rising beyond its rating. The protection system trips to turn off the inverter. This operation is expected as it is observed in the frequency domain analysis and the simulation. Now R_v is set to 15 Ω. An experiment is carried out for this weak grid, and the resultant experimental waveforms are shown in Fig. 7(c). As it can now be seen that the inverter is stable, which proves the theoretical analysis of this work. Thus, the redesigned parameter using the impedance-based method ensures the stability and robustness of the inverter when connected in weak grids.

V. Conclusion

This paper presents the impedance modeling and the impedance-based stability analysis of the UDC inverter. The dq-impedance of the UDC inverter is derived analytically, which is verified by simulation. Both the d- and q-axis impedance show the resistive behavior at the fundamental frequency, which shows a better stability property compared to the traditional control technologies. The derived impedance model is used to determine the stability of the grid-connected UDC inverter. The analysis has been used in designing the grid-tied UDC inverter parameter to operate in a weak grid condition.

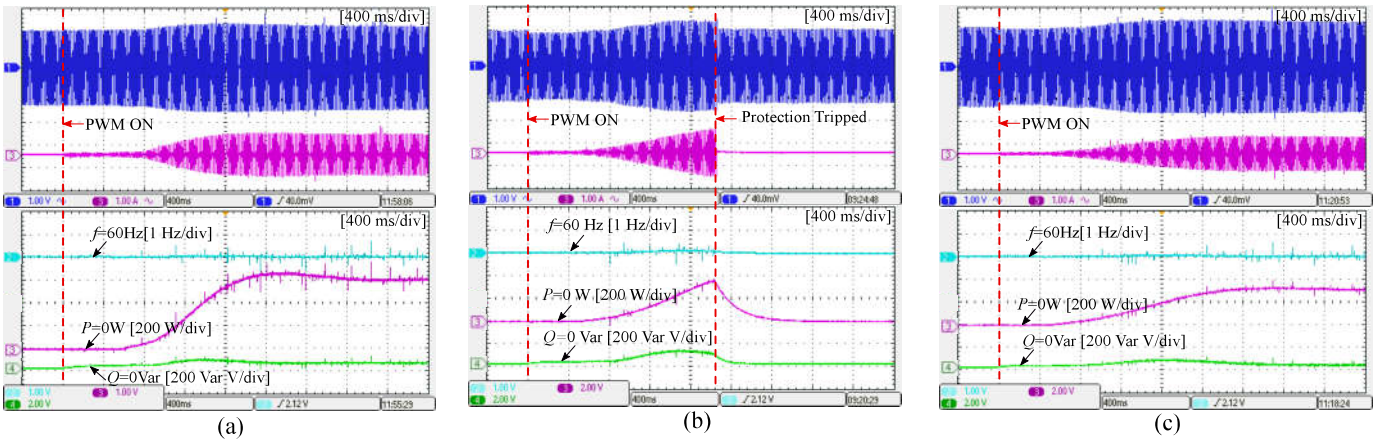

Fig. 7. Experimental results for different scenarios of the grid condition and parameters: (a) a strong grid, stable system, (b) a weak grid, unstable system and (c) a weak grid, stable system with redesigned parameter.

REFERENCES

[1] K. Visscher and S. D. Haan, "Virtual synchronous machines (VSG's) for frequency stabilisation in future grids with a significant share of decentralized generation," in *Proc. of IET-CIRED Seminar on Smart Grids for Distribution*, 2008, pp. 1–4.

[2] W. Wu, Y. Chen, A. Luo, L. Zhou, X. Zhou, L. Yang, Y. Dong, and J. M. Guerrero, "A virtual inertia control strategy for dc microgrids analogized with virtual synchronous machines," *IEEE Trans. Ind. Electron.*, vol. 64, no. 7, pp. 6005–6016, July 2017.

[3] A. D'Arco and J. R. Suul, "Equivalence of virtual synchronous machines and frequency-droops for converter-based microgrids," *IEEE Trans. Smart Grid*, vol. 5, no. 1, pp. 394–395, 2014.

[4] S. D'Arco, J. A. Suul, and O. B. Fosso, "A virtual synchronous machine implementation for distributed control of power converters in smartgrids," *Electric Power Systems Research*, vol. 122, pp. 180–197, 2015.

[5] Q.-C. Zhong, "Virtual synchronous machines: A unified interface for smart grid integration," *IEEE Power Electronics Magazine*, vol. 3, no. 4, pp. 18–27, Dec 2016.

[6] Q.-C. Zhong and Y. Zeng, "Universal droop control of inverters with different types of output impedance," *IEEE Access*, vol. 4, pp. 702–712, Jan. 2016.

[7] Q.-C. Zhong, W. L. Ming, and Y. Zeng, "Self-synchronized universal droop controller," *IEEE Access*, vol. 4, pp. 7145–7153, Oct. 2016.

[8] Q.-C. Zhong, "Robust droop controller for accurate proportional load sharing among inverters operated in parallel," *IEEE Trans. Ind. Electron.*, vol. 60, no. 4, pp. 1281–1290, Apr. 2013.

[9] M. Amin, Q.-C. Zhong, L. Zhang, Z. Li, and M. Shahidehpour, "Small-signal modeling and analysis of vsm for distributed generation in a weak grid," in *IECON 2018 - 44th Annual Conference of the IEEE Industrial Electronics Society*, Oct 2018.

[10] P. S. Kundur, *Power System Stability and Control*. New York: Mc-Graw-Hills, 1994.

[11] J. Beerten, S. D'Arco, and J. A. Suul, "Identification and small-signal analysis of interaction modes in vsc mtdc systems," *IEEE Trans. Power Del.*, vol. 31, no. 2, pp. 888–897, April 2016.

[12] M. Amin, J. A. Suul, S. D'Arco, E. Tedeschi, and M. Molinas, "Impact of state-space modelling fidelity on the small-signal dynamics of vsc-hvdc systems," in *11th IET International Conference on AC and DC Power Transmission*, Feb 2015, pp. 1–11.

[13] T. Hu, "A nonlinear-system approach to analysis and design of power-electronic converters with saturation and bilinear terms," *IEEE Trans. Power Electron.*, vol. 26, no. 2, pp. 399–410, Feb 2011.

[14] R. D. Middlebrook, "Input filter considerations in design and application of switching regulators," in *1976 IEEE Ind. Appl. Soc. Annu. Meeting*, 1976, pp. 366–382.

[15] J. Sun, "Impedance-based stability criterion for grid-connected inverters," *IEEE Trans. Power Electron.*, vol. 26, no. 11, pp. 3075–3078, Nov 2011.

[16] M. Amin and M. Molinas, "Small-signal stability assessment of power electronics based power systems: A discussion of impedance- and eigenvalue-based methods," *IEEE Trans. Ind. Appl.*, vol. 53, no. 5, pp. 5014–5030, Sep. 2017.

[17] J. Huang, K. A. Corzine, and M. Belkhayat, "Small-signal impedance measurement of power-electronics-based ac power systems using line-to-line current injection," *IEEE Trans. Power Electron.*, vol. 24, no. 2, pp. 445–455, Feb 2009.

[18] G. Francis, R. Burgos, D. Boroyevich, F. Wang, and K. Karimi, "An algorithm and implementation system for measuring impedance in the d-q domain," in *2011 IEEE Energy Conversion Congress and Exposition*, Sep. 2011, pp. 3221–3228.